Definition of a nanoindentation-based methodology to optimize process parameters of coating deposition on silicon wafer

Available online at www.sciencedirect.com

ScienceDirect

Procedia CIRP 138 (2026) 1055–1060

www.elsevier.com/locate/procedia

18th CIRP Conference on Intelligent Computation in Manufacturing Engineering

Definition of a nanoindentation-based methodology to optimize process parameters of coating deposition on silicon wafer

Maurizio Galetto*, Gianfranco Genta, Giacomo Maculotti, Lorenzo Giorio, Giovanni Marchiandi

Department of Management and Production Engineering, Politecnico di Torino, C.so Duca degli Abruzzi 24, 10129 Turin, Italy

* Corresponding author. Tel.: +39-011-090-7224; *E-mail address:* maurizio.galetto@polito.it

Abstract

Semiconductor industry drives energy, IT, and physics research and silicon technology is crucial in photovoltaic panels, chips, boards, e-mobility batteries, and infrared vision. Surface technologies enhance silicon functionality: coatings boost solar cell efficiency, panel passivation, and biomedical integration. Coatings like SiO_2 and polycrystalline silicon bolster surface hardness for packaging and transport. Various industrially available deposition methods demand metrological control, often underexplored. This study proposes a cost-effective nanoindentation-based method to assess coating surface integrity leveraging on mechanical properties, thickness-related gradients. Results are complemented by topographical and AFM inspections. The method is applied to Chemical Vapor Deposition of SiO_2/Si<100> investigating gas-ratio effect.

Peer-review under responsibility of the scientific committee of the 18th CIRP Conference on Intelligent Computation in Manufacturing Engineering (CIRP ICME ‘24)

Keywords: Surface integrity; Coating; Silicon

1. Introduction

The semiconductor industry is strategic worldwide, due to critical applications in energy, information technology (IT) and fundamental physics research. Silicon, amongst the others, covers a relevant market share thanks to its core applications in photovoltaic panels, general applications for chips and printed circuit boards (PCBs), batteries for e-mobility and infra-red vision. In fact, Silicon technology can be considered an enabling technology for advanced communication and protocols [1], e.g. for 5G antennas and for integrated circuits (ICs) aimed at controlling wave signals at high frequencies, i.e. up to 100 GHz [2]. Similarly, for vehicles electrification towards a sustainable transportation circulating fleet, silicon (Si) and silicon carbide (SiC) are deployed for power semiconductor devices, i.e. insulated-gate bipolar transistors (IGBTs), MOSFETs and Diodes, in power modules for inverter, DC-DC converter, and chargers [3,4]. Furthermore, silicon finds applications in photonics for long-wave infra-red (8 µm to 14 µm) vision thermos-cameras, often exploited in physics, aerospace, military, but often multilayer system, as silicon nitride (Si_3N_4), silicon dioxide (SiO_2), SiC are required, or amorphous silicon (aSi) [5,6]. Polymeric coatings have been suggested to aid biological integration of medical electronic devices for which silicon is used for ICs and micro power sources [7], or to reduce surface adhesion to improve durability for Micro Electro-Mechanical Systems (MEMS) [8]. Last, but not the least, Silicon is most often exploited in energy harvesting devices and energy generation devices, e.g. photovoltaics panels (PVs). PVs market is still dominated by Si wafers technology, even though semiconductor research has focused on surface technology to engineer performances [9]. Si wafer manufacturing is critical, and often surface technologies are

Peer-review under responsibility of the scientific committee of the 18th CIRP Conference on Intelligent Computation in Manufacturing Engineering (CIRP ICME ‘24)
10.1016/j.procir.2026.01.182

exploited to coat the functional surface to enhance properties. Antireflection coatings increases solar cells efficiency by enabling broadband light trapping, and texturing such coatings, e.g. by wrinkles, can increase the efficiency of almost 15% [10]. TiO_2 coating has been shown to improve surface passivation that is critical in solar panels [11]. Silicon dioxide [9] and polycrystalline silicon [12] can be used to engineer the hardness of the surface for packaging and transportation, as well as being beneficial for passivation [13]. Several deposition methods are available, e.g. physical vapour deposition (PVD) [14], chemical vapour deposition (CVD) [15], spin coating electrospray [16], and tuning relevant process parameters is a challenging procedure scarcely investigated in the literature. Most often, study and optimization of process parameters are not reported in regard to their effect on the surface coating properties.

This work proposes to study the effect of process parameters on topographical and mechanical properties of Si wafer for PVs application thin coatings basing on nanoindentation. Results are correlated with process parameters investigated in the operating range of the deposition process.

The methodology is applied to a case study considering Atmospheric Pressure Chemical Vapour Deposition of silicon dioxide on a silicon wafer.

2. Methodology

2.1. Manufacturing setup

Atmospheric Pressure Chemical Vapour Deposition (APCVD) is a process used to deposit thin films onto a substrate by reacting vapor-phase chemicals at atmospheric pressure. Fig. 1 shows the schematic of APCVD to deposit SiO_2 on Si wafers. The process requires input of silane gas (SiH_4) and oxygen (O_2) at a certain volumetric ratio, i.e. $r = {v_{SiH_4}}/{v_{O_2}}$. The reaction to create SiO_2 also depends on the substrate temperature, which, along with the speed of the conveyor belt, affects the thickness of the resulting thin layer.

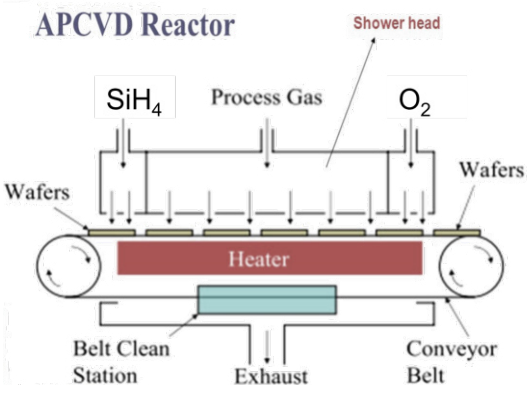

Fig. 1 APCVD process scheme for depositing SiO_2 on Si wafers.

This work focuses on the effect of the gas volumetric ratio r to study its effect with respect to standard industrial manufacturing conditions. In particular, two alternative conditions are investigated, i.e. $r = \{{1}/{20}, {1}/{25}\}$. Other process parameters are not reported for confidentiality of the manufacturing company. The nominal thickness of the coating is 500 nm. The substrate was a wafer of Si<100>, and the control quality variable that are considered are: the surface topography, the film thickness t and the surface mechanical response.

The characterizations were performed in the metrological room of Mind4Lab at Department of Management and Production Engineering of Politecnico di Torino on the two coatings and on the substrate.

2.2. Surface topography characterization

Surface topography was measured by means of a Zygo NewView9000 Coherence Scanning Interferometer (CSI) [17], see Fig. 2(a). The CSI was calibrated [18] with a measurement noise of 10 nm [19] Measurements were performed in 6 random locations with a 20× magnification objective (numerical aperture of 0.4, with a square field of view of (0.43×0.43) mm×mm and a square pixel having a side of 0.43 µm). The surface topography was characterized according to ISO 25178-2 and ISO 25178-3 [20,21] by evaluating the surface areal field height parameters on the scale limited (SL) surface obtained with standard bandwidth specification of N_{is} and N_{ic} of 2 µm and 0.2 mm, respectively. The two bandwidth specifications represent, respectively, the cut-off of the S-filter, i.e. a high-pass (in the spatial wavelength) filter applied to remove effect of lateral sampling and noise, and the L-filter, which is a low-pass filter to remove the waviness of the surface. Both filters are applied as Gaussian filters [22]. An F-operator to remove the nominal planar shape of the surface was applied by least-square fitting the measured surfaces [20,21]. No measurement disturbances were identified thus eliminating an analysis step liable of distorting measurements [23].

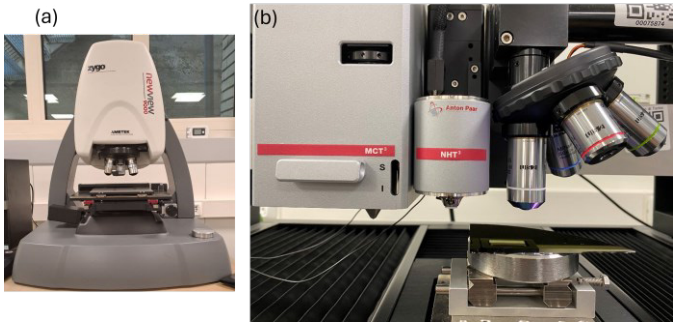

Fig. 2 (a) Zygo NewView9000 CSI and (b) Anton Paar NHT^3 nanoindenter.

2.3. Surface mechanical response characterization

Surface mechanical characterization was performed by nanoindentation [24] by means of an Anton Paar STeP6 platform equipped with the NHT^3, see Fig. 2 (b), head featuring a three plate conductive sensor for force and displacement with force and displacement noise of 1% and 0.5%, respectively. The characterization considers two approaches.

The first, conventional quasi-static loading-holding-unloading (each of 60 s) force cycles [25] at a maximum load

of 0.5 mN. Characterization is reported in terms of indentation hardness, H_{IT}, and the indentation modulus, E_{IT}, that estimates the Young's modulus as average and standard deviation of 16 indentations (performed on each sample).

The second, a set of continuous multi cycle indentations (CMC) were performed to study the evolution of the mechanical properties as a function of depth. CMC consists of applying replicated quasi-static indentations with increasing maximum load in the same location of the surface. In so doing, the unloading of each subsequent indentation corresponds to an increasing maximum penetration depth, h_{max}, at which the mechanical characterization is performed [26]. Five CMC indentations with 15 cycles ranging from 0.25 mN to 100 mN, quadratically spaced, were performed.

The indentation platform frame compliance and Berkovich indenter geometry were calibrated [27], with a relative measurement uncertainty of 10% on H_{IT} and of 4% on E_{IT} [28].

Thickness measurements are performed by relying on CMC indentation results, by means of statistical deconvolution of the mechanical response [29,30].

2.4. Atomic Force Microscopy

Additional measurements by means of Atomic Force Microscopy (AFM) to assess topographic homogeneity and adhesion forces were carried out by means of a tapping-mode measurement of a (40×40) µm×µm area by means of a NanoWorld rectangular section arrow-tip (radius of 10 nm and half-cone angle of 10°). Each measurements were performed with a resolution of 400 lines. Due to the long measurement time, only one measured area per wafer was measured, and only the coated surface was inspected.

Topography was then processed by first applying tip deconvolution, levelling and evaluating SL-surface (N_{is} and N_{ic} of 0.5 µm and 25 µm, respectively).

Five measurements of force-distance curves were performed on random positions of the measured surfaces to evaluate snap-in and adhesion points.

3. Results and Discussion

3.1. Surface topography characterization

Surface topography of SiO2/Si<100> deposited with the two different gas ratios was measured by the CSI. Fig. 3 shows the qualitative appearance of the two measured surfaces. As it can be appreciated, very limited differences qualitatively can be distinguished on the surface topography, which presents some wide shallow valleys.

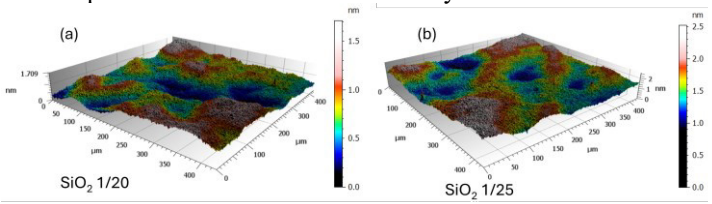

Fig. 3 Surface topography measured by CSI of SiO_2/Si<100> deposited with a gas ratio of (a) 1/20 and (b) 1/25.

The results of the quantitative characterization are reported in Table 1. As it can be appreciated, the coating obtained with the gas ratio of 1/25 shows a rougher surface both in terms of *Sa*, *Sq* and *Sv* and *Sz*. The larger average is statistically significant with a risk of error of 5%, when tested with a *t*-test. The results of the higher central statistical moments, i.e. the skewness *Ssk* and the kurtosis *Sku*, show that the topographies can be considered normally distributed, for they are not statistically different from the values of 0 and 3, respectively.

Table 1 CSI Characterization of the SL-surface for the SiO_2 coating with the two gas ratios. Mean and uncertainty evaluated as reproducibility with a coverage factor of k=2.

	Sa / nm	*Sq* / nm	*Ssk* / -	*Sku* / -	*Sv* / nm	*Sz* / nm
1/20	0.2±0.08	0.3±0.11	0.5±0.3	2.9±0.3	1.0±0.4	2.0±0.3
1/25	0.3±0.05	0.3±0.06	-0.1±0.3	4.2±4.6	2.8±4.5	4.1±4.3

3.2. Surface mechanical characterization

Nanoindentations were performed to characterize the coating and provide relative information of indentation hardness and modulus with respect to the base material.

Fig. 4 shows the indentation curves. As it can be qualitatively appreciated, the SiO_2 coating allows for a deeper penetration depth with respect to the base material.

Quantitative characterization is reported in Fig. 5, which shows the interval plots of the H_{IT} and E_{IT} on the three considered materials. As it can be appreciated, the different dispersion of the three characterization suggests a systematic effect of the material not only on the average, but also on the standard deviation of the evaluated mechanical parameter.

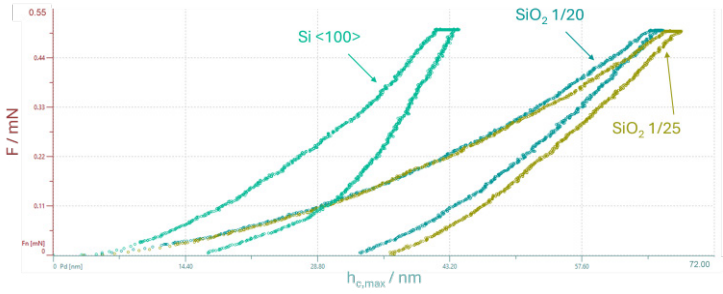

Fig. 4 Indentation Curve, *F(h)*, for the three considered materials: the Si<100> substrate and the two SiO_2 coatings.

Accordingly, a Bonferroni hypothesis test of heteroscedasticity was performed [31]. The test showed that, only for H_{IT}, the standard deviation is affected by the material, at a confidence level of 95%. This is consistent with the well-known greater sensitivity and uncertainty of the indentation hardness to surface integrity [28]. In fact, the greater roughness of the SiO_2 coating deposited with a gas ratio of 1/25 (see Section 3.1) resulted in a more dispersed mechanical characterization.

A 1-way Analysis of Variance (ANOVA) was then performed to test the effect of the material on the average mechanical response. The ANOVA (performed using

assumptions for heteroscedasticity [31] and with a confidence level of 95%), as it can be appreciated qualitatively in Fig. 5, showed a systematic effect of the SiO_2 coating in reducing both hardness and elasticity with respect to the base material, whose response is consistent with other values reported in the literature and whose greater dispersion can also be motivated by relative orientation between the crystalline orientation and the indenter [32]. Conversely, no effect introduced by the gas ratio could be highlighted on the mechanical response of the SiO_2.

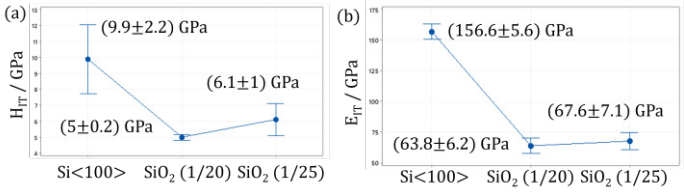

Fig. 5 Mechanical characterisation of substrate and coating. Interval plots with error bars at 95% confidence level computed with individual standard deviation.

It is worth noting that the area between the loading and unloading portion represents the plastic work of indentation. Consistently with the coating hardness smaller than the substrate, a greater plastic deformation results on the coating which is though partially compensated by its lower E_{IT}. However, the overall work of indentation for the SIO_2 coating is still greater, (11.8±1.2) pJ, than the one of the Si<100>, (8.3±1.4) pJ, due to the discontinuity that can be appreciated in the end portion of the unloading of the Si<100> (see Fig. 5) that can be ascribed to partial recovery of phase transformation [33].

Last, characterization results obtained by CMC indentations are reported and discussed. Fig. 6(a,c) shows the evolution of the indentation modulus E_{IT} as a function of maximum penetration depths for subsequent cycles. As it can be appreciated, moving from the coating towards the substrate a progressive stiffening of the material is apparent and results from the convolution of the mechanical response of the coating layer and the substrate. This convolution induces and apparent stiffening [29,30,34] of the response.

By deconvoluting the mechanical response, that can be modeled as a gaussian mixture model [30] the evaluation of the coating thickness can results by means of a cost-effective approach, i.e. nanoindentation rather than, for example X-ray diffractometry. The measured thickness resulted of (535±72) nm and of (542±84) nm for the 1/20 and 1/25 gas ratio, respectively.

What is here most interesting to report is that, for both the gas ratio conditions, the SiO_2 coating showed two alternative responses. The first, see Fig. 6(a-b), is a progressive, but continuous, evolution of E_{IT} which corresponds to conventional indentation curves with no particular features. The second, Fig. 6(c-d), is instead associated with a cracking of the coating that can be detected by the pop-in, i.e. the depth discontinuity, event in the indentation curve, shown in Fig. 6(d). The cracking takes place at depths near the coating thickness, i.e. where there is a geometrical discontinuity of the material. Furthermore, it is relevant to notice that such cracking was more frequently observed in the coating deposited with a 1/25 gas ratio, which also presented a rougher surfaces with more valleys, liable of weakening the coating.

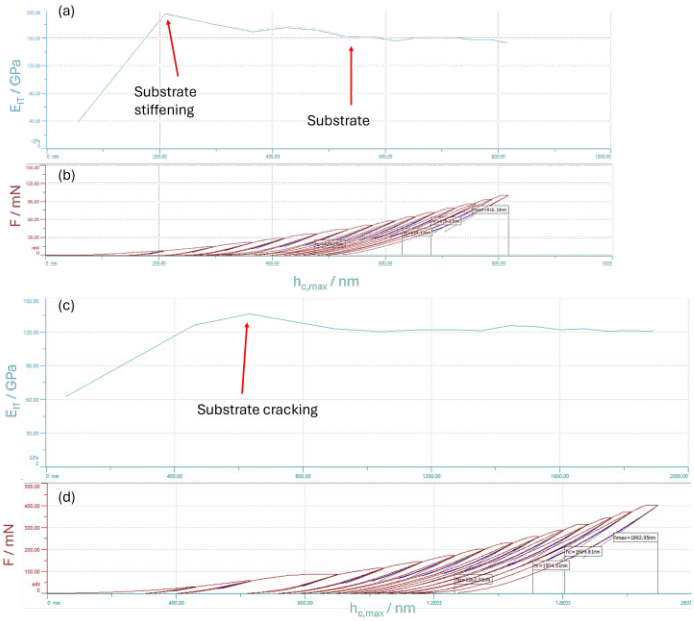

Fig. 6 Continuous Multi Cycle nanoindentation results. Modes of mechanical response. (a, c) E_{IT} as a function of penetration depth and (b, d) indentation curves F(h). (a-b) non-cracking response, (c-d) cracking response with sudden event of pop-in in (d).

3.3. Atomic Force Microscopy

Surface topography and phase measured by means of tapping AFM are shown in Fig. 7. Consistently with CSI measurements (Section 3.1) the deposition with 1/25 gas ratio is qualitatively rougher, which is well reflected by phase measurements, see Fig. 7(b,d). Surface topography characterization results in relative roughness assessment coherent with those obtained with the CSI (see Table 1), with values of *Sa* of 0.526 nm and of 0.757 nm and of *Sq* of 0.697 and of 1.002 nm, respectively for the deposition with a volumetric gas ratio of 1/20 and 1/25.

Phase measurement allows to highlight great local homogeneity of the material with no particular inhomogeneities and density change related to the material deposition.

Finally, the characterization of the Force-distance curve allows insights on the local adhesion. Sample curves measured on the two coatings are shown in Fig. 8. The distance axes represents the separation between the cantilever tip and the surface, as the tip travel corrected for the deflection and the baseline offset. The discontinuities in the approach and retract force curve allow identifying, respectively, the snap-in and the adhesion event. These indicate the point when atomic forces starts attracting the tip, and the point when Van-der-Waals forces are overcome by the cantilever travel. Results, reported in Table 2, show that smaller distances and larger (in magnitude) forces are associated with the coating deposited with a gas ratio of 1/25. This is consistent with the greater roughness inducing a larger adhesion for the coating.

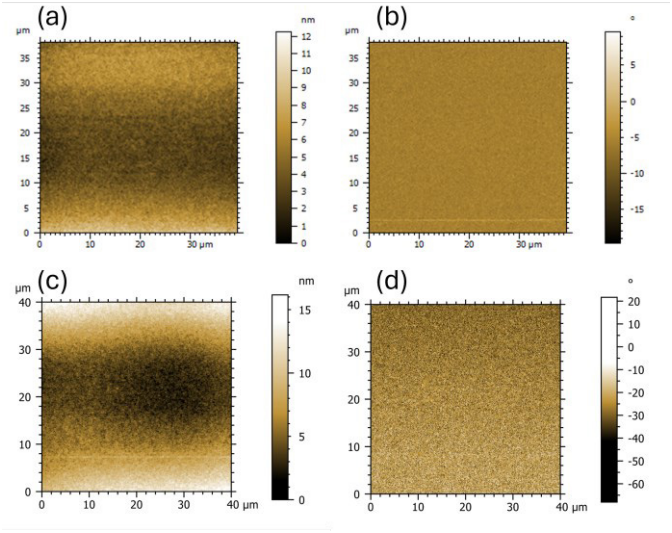

Fig. 7 AFM tapping measurement. SiO_2/Si<100> deposited with a gas ratio of 1/20 (a) topography and (b) phase, and of 1/25 (c) topography and (d) phase.

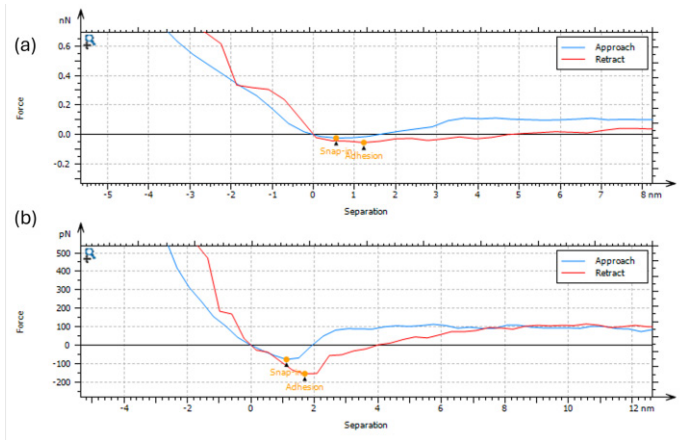

Fig. 8 Force-distance curve on SiO_2/Si<100> deposited with a gas ratio of (a) 1/20 and (b) 1/25. The more representative separation scale is reported.

Table 2 Force-adhesion characterisation of the two coating. Values of snap-in and adhesion in force and tip-surface separation

Coating	Snap-in	Adhesion
1/20	(50.89±200) nm (-34.01±15.6) pN	(99.96±26.9) nm (-61.08±46.5) pN
1/25	(56.82±62.4) nm (-55.88±50.0) pN	(1.34±0.7) nm (-132.5±65.7) pN

4. Conclusions

This work proposed a study of surface topographical and mechanical properties of a silicon dioxide coating deposited via atmospheric pressure chemical vapour deposition on a silicon wafer substrate for photovoltaic panels. The work focused on the investigation of the silane to oxygen gas ratio on the coating response. Results showed that the coating, although allowing for increased passivation, reduces, in average, the hardness of the surface. The considered process parameter does not affect the average surface mechanical response but significantly affects the topography and the higher gas ratio induces a rougher and richer in valleys topography liable of introducing geometric singularities liable of locally weakening the coating surface. Investigation by Atomic Force Microscopy allowed insights on the topography, which also at a smaller scale confirmed the greater roughness induced by the larger gas ratio, proving an homogeneous material deposition, and highlighting how the rougher surface is characterized by greater adhesion forces. Future works will focus on extending the scope of the process parameters effect and correlating with relevant functional properties for applications on energy industry.

Acknowledgements

This work has been carried out within the project 22RPT01 TracInd BVK-H which has received funding from the European Partnership on Metrology, cofinanced from the European Union's Horizon Europe Research and Innovation Programme and by the Participating States.

References

[1] Lin J-J, Wu H-T, Su Y, Gao L, Sugavanam A, Brewer JE, Kenneth KO. Communication Using Antennas Fabricated in Silicon Integrated Circuits. IEEE J Solid-State Circuits 2007;42:1678–87.
[2] Gu X, Liu D, Sadhu B. Packaging and Antenna Integration for Silicon-Based Millimeter-Wave Phased Arrays: 5G and Beyond. IEEE J Microwaves 2021;1:123–34.
[3] Di Giovanni F. Silicon Carbide: Physics, Manufacturing, and its role in Large-Scale Vehicle Electrification. Chips 2023;2:209–22.
[4] Smith D, Ozpineci B, Graves R, Jones PT, Lustbader J, Kelly K, Walkowicz K, Birky A, Payne G, Singler C, Mosbacher J. Medium- and Heavy-Duty Vehicle Electrification: An Assessment of Technology and Knowledge Gaps. Oak Ridge, TN (United States): 2020.
[5] Khandekar C, Jin W, Fan S. Nanophotonic detector array to enable direct thermal infrared vision. Opt Express 2022;30:39222.
[6] Patel M, Karamalidis AK. Germanium: A review of its US demand, uses, resources, chemistry, and separation technologies. Sep Purif Technol 2021;275:118981.
[7] Ziemba AM, Woodson MCC, Funnell JL, Wich D, Balouch B, Rende D, Dahkia NA, Bao J, Oprea I, Cao D, Bajalo N, Ereifej SE, Capadona JR, Palermo EF, Gilbert RJ. Development of a Slow-Degrading Polymerized Curcumin Coating for Intracortical Microelectrodes. ACS Appl Bio Mater 2023;6:806–18.
[8] Katiyar JK, Mohammed AS. Physical, tribological and mechanical properties of polymer composite coating on silicon wafer. Tribol Int 2022;165:107307.
[9] Arul Prishya AS, Chopra L, Manikanika. Comprehensive review on uses of silicon dioxide in solar cell. Mater Today Proc 2023;72:1471–8.
[10] Zhang Y, Zheng J, Fang C, Li Z, Zhao X, Li Y, et al. Enhancement of silicon-wafer solar cell efficiency with low-cost wrinkle antireflection coating of polydimethylsiloxane. Solar En Mater Solar Cells 2018;181:15–20.
[11] Richards BS, Cotter JE, Honsberg CB. Enhancing the surface passivation of TiO2 coated silicon wafers. Appl Phys Lett 2002;80:1123–5.
[12] Yan D, Cuevas A, Michel JI, Zhang C, Wan Y, Zhang X, Bullock J. Polysilicon passivated junctions: The next technology for silicon solar cells? Joule 2021;5:811–28.
[13] Yan D, Cuevas A, Stuckelberger J, Wang EC, Phang SP, Kho TC, Michel JI, Macdonald D, Bullock J. Silicon solar cells with passivating contacts: Classification and performance. Prog Photovoltaics: Res Applic 2023;31:310–26.

[14] Cannon P, McGlynn E, Freeland B, Gaughran J. Development and optimisation of a SiO 2 PVD technique based on the thermal decomposition of PDMS. New Journal of Chemistry 2023;47:3734–44.
[15] Foggiato J. Chemical Vapor Deposition of Silicon Dioxide Films. Handbook of Thin Film Deposition Processes and Techniques, Elsevier; 2001, p. 111–50.
[16] Cherkouk C, Rebohle L, Skorupa W, Strache T, Reuther H, Helm M. Spraying spin coating silanization at room temperature of a SiO2 surface for silicon-based integrated light emitters. J Colloid Interface Sci 2009;337:375–80.
[17] de Groot P. Coherence Scanning Interferometry. In: Leach RK, editor. Optical Measurement of Surface Topography, Berlin: Springer-Verlag; 2011, p. 187–208.
[18] ISO 25178-604:2013 Geometrical Product Specification (GPS) - Surface texture: Areal Part 604: Nominal characteristics of non-contact (coherence scanning interferometry) instruments. ISO, Genève.
[19] Giusca CL, Leach RK, Helary F, Gutauskas T, Nimishakavi L. Calibration of the scales of areal surface topography measuring instruments: part 1. Measurement noise and residual flatness. Meas Sci Technol 2012;23:065005.
[20] ISO 25178-2:2021 Geometrical product specifications (GPS) — Surface texture. Areal Part 2: Terms, definitions and surface texture parameters. ISO, Genève.
[21] ISO 25178-3:2012. Geometrical product specifications (GPS) — Surface texture : Areal Part 3 : Specification operators. ISO, Genève.
[22] Maculotti G, Feng X, Su R, Galetto M, Leach R. Residual flatness and scale calibration for a point autofocus surface topography measuring instrument. Meas Sci Technol 2019;30:075005.
[23] Maculotti G, Genta G, Quagliotti D, Galetto M, Hansen HN. Gaussian process regression-based detection and correction of disturbances in surface topography measurements. Qual Reliab Eng Int 2022;38:1501–1518.
[24] Lucca DA, Herrmann K, Klopfstein MJ. Nanoindentation: Measuring methods and applications. CIRP Ann Manuf Technol 2010;59:803–19.
[25] ISO 14577-1:2015 Metallic materials-Instrumented indentation test for hardness and materials parameters - Part 1: Test method. ISO, Genève.
[26] Maculotti G, Goti E, Genta G, Mazza L, Galetto M. Comprehensive mechanical and tribological characterization of metal-polymer PTFE+Pb/Bronze coating by in-situ electrical contact resistance measurement augmented tribo-mechanical tests. Tribol Int 2024;193:109397.
[27] Galetto M, Genta G, Maculotti G. Single-step calibration method for nano indentation testing machines. CIRP Annals 2020;69:429–32.
[28] Maculotti G, Genta G, Galetto M. An uncertainty-based quality evaluation tool for nanoindentation systems. Measurement 2024;225:113974.
[29] Puchi-Cabrera ES, Staia MH, Iost A. Modeling the composite hardness of multilayer coated systems. Thin Solid Films 2015;578:53–62.
[30] Genta G, Maculotti G. Thin coatings thickness measurement by augmented nanoindentation data fusion. CIRP Ann Manuf Technol 2024;73:Accepted for publication.
[31] Montgomery D, Runger G, Hubele N. Engineering statistics. New York: John Wiley & Sons Inc.; 2010.
[32] Hopcroft MA, Nix WD, Kenny TW. What is the Young's modulus of silicon? Journal of Microelectromechanical Systems 2010;19:229–38.
[33] Ruffell S, Bradby JE, Fujisawa N, Williams JS. Identification of nanoindentation-induced phase changes in silicon by in situ electrical characterization. J Appl Phys 2007;101:1–7.
[34] Bull SJ. Nanoindentation of coatings. J Phys D Appl Phys 2005;38:R393